Indian Journal of Biochemistry & Biophysics
Vol. 63, April 2026, pp. 369-388
DOI: 10.56042/ijbb.v63i4.18046

Computational vibrational analysis, electronic properties and molecular docking of 1-cyclohexanol and 2- (3-methyl-1, 3-butadienyl) -1, 3, 3-Trimethyl: A DFT approach

Govindu Reddy Dagada[1], Vijayalakshmi Duraikannu[1]*, Rajesh Punniyamoorthy[1], Anbarasu Mariyappillai[2], Kayashrini Sundaramoorthi[1] & Jesuraj Kabiriyel[3]

[1]Department of Physics, School of Basic Science; & [2]Department of Agronomy, School of Agriculture, Vels Institute of Science and Technology & Advanced Studies, Pallavaram, Chennai-603 203, Tamil Nadu, India

[3]Department of Condensed Matter Physics, Saveetha School of Engineering, Saveetha Institute of Medical and Technical Sciences (SIMATS), Chennai-602 105, Tamil Nadu, India

Received 19 March 2025; *revised 24 April 2025*

The present investigation employed density functional theory (DFT) at the B3LYP/6-311++ (d, p) level of theory to examine the terpenoid molecule 1- Cyclohexanal, 2- (3-methyl-1, 3-butadienyl) -1, 3, 3-trimethyl (3MBD-TMC). A thorough vibrational investigation was carried out to confirm vibrational modes, including FT-IR spectrum assignments and PED calculations. To understand the electronic transitions, the UV-visible absorption spectra were examined. The HOMO-LUMO gap, in particular, sheds light on the electronic stability and reactivity of the molecule. The charge distribution has been demonstrated using molecular electrostatic potential (MEP) mapping, and further information on the electron density across the molecule was provided by Mulliken charge analysis. In order to investigate the electron delocalization, intramolecular and intermolecular interactions were performed through Natural Bond Orbital (NBO) analysis. To help with the understanding of chemical reactivity, the nucleophilic and electrophilic sites were evaluated using the Fuki function. Furthermore, the nature of bonding and electron localization inside the molecule was examined using the computation of the LOL (Localized Orbital Locator) and ELF (Electron Localization Function). A detailed examination of non-covalent interactions was given by Reduced Density Gradient (RDG) analysis, which supported molecular docking experiments that looked at 8D58 protein interpreted to the possible binding affinity of 3MBD-TMC with biological targets by Ramachandran plots. Future research on the possible biological and pharmacological uses of 3MBD-TMC will benefit from the comprehensive understanding of its structural, electronic, and vibrational properties provided by the combined theoretical and computational results.

Keywords: Cyclohexanone, ELF, LOL, Mulliken charge, Vibrational assignments

Cancer has been a continuing difference of opinion around the world resulting in preventive therapies and the discovery of cures in recent times[1]. From the literature review, cyclohexanone derivatives are linked with patterns of biological activities including antimalarial, anti-inflammatory, anti-cancer, antiasthmatic, antibacterial, antihypertensive, and also blood platelet anti-aggregating activity[2]. The purpose of this research was to assess the anticancer properties of 1-Cyclohexanol, 2- (3-methyl-1, 3-butadienyl) -1, 3, 3-trimethyl-derivative products in human colon cancer cells[3]. The anticancer properties of cyclohexanol molecules have been demonstrated. The outstanding antibacterial effect is caused by active groups attached to the cyclohexanal ring[4]. Two basic compounds with methyl and butadienyl groups are synthesized as an example, and the butadienyl-based complexes show positive cytotoxic activity in liver tumorcells[5]. The chemical formula of cyclohexanone is $C_{14}H_{24}O$ and its molecular weight is 208.18 g/mol. This colorless molecule contains a functional group called a ketone. The literature review indicates that no reports on the chemical cyclohexanone have been found in theoretical DFT, spectroscopic, and molecular docking studies. Initially, the GC-MS technique is applied to confirm the structure and stability. To analyze the compound FT-IR and UV-Visible spectroscopy, the method has been followed. DFT/B3LYP method computations employing the 6-311++G (d, p) basis set were utilized to understand the optimized structure geometry and harmonic frequency of the 3MBD-TMC component. The HOMO LUMO energy gap of the 3MBD-TMC molecules is carried out. The intra- and intermolecular

*Correspondence:
E-mail: viji.duraikannu@gmail.com

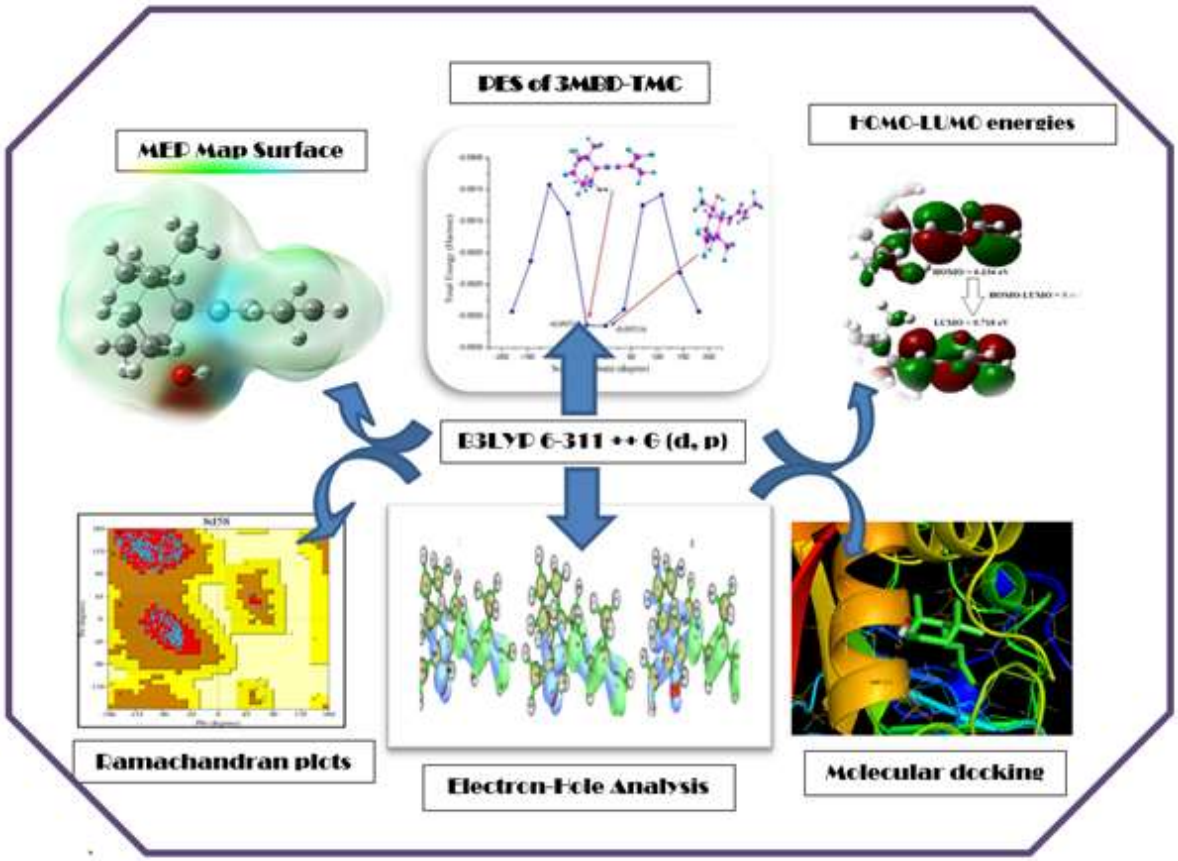

Graphical abstract

interactions of hydrogen bonding and charge delocalization of the title compound were analyzed by NBO[6]. The topological factors ELF, LOL, RDG and Electron Hole Analysis of 3MBD-TMC possess the understanding of the localization of the electrons, holes, density and non-covalent properties of it. In molecular docking interpreted with 8D58 protein to 3MBD-TMC ligand, which exhibits possible binding affinity, express the biological targets through Ramachandran plots[2].

Experimental techniques detail

Using the Soxhlet procedure and a review of the literature, the *Hybanthus enneaspermus* crude was investigated using the Gas Chromatography-Mass Spectrometry (GC–MS) technology (QP2010 Plus – Shimadzu). The MS non-polar capillary column, measuring 30 m in length, 0.25 mm in inner diameter, and 0.25 m in thickness, is coated with polydimethylsiloxane. It is then heated to 250°C, and the GC–MS spectra show a region of 25 min. The GC-MS data revealed the presence of a biomolecule. Based on its anti-cancer properties, we specifically chose one quantifiable phytochemical molecule (3MBD-TMC) for more study, and we bought a 99% pure 3MBD-TMC chemical from the Sigma-Aldrich Company[7]. The 3MBD-TMC sample was evaluated using FT-IR spectrum analysis in the recorded region of 4000 – 400 cm^{-1}. Using a Perkin Elmer FT-IR spectrophotometer with the KBr pellet method and a spectral solution comprising 4.0 cm^{-1}, the spectrum was measured at room temperature. The wavelength range of the measured UV–vis spectrum is 300–100 nm, with UV-3600 plus. A quartz cell with a diameter of 1 cm and a slit width of 0.5 nm is used by Shimadzu Instrument[8]. In Kattankulathur, Chengalpattu district, Tamil Nadu, India, the SRM College of Science recorded the GC-MS, FT-IR, and UV-vis spectra results.

Computational Methods

DFT, a popular tool for computational quantum mechanical modeling, can be used to analyze the electrical structure of many-body systems. All theoretical computations in this paper were performed using the Gaussian 09W program. The compound was

depicted using the ChemCraft 1.8 and Gauss View 5.0 software approach. Using the NBO 3.1 program in the Gaussian 09W atthe B3LYP/6-311 ++ G (d, p) method, the NBO analysis was completed. The ones listed above are used to determine the molecular electrostatic potential (MEP), which is then used to assess the reactive sites (the charged section of a molecule). The molecular docking calculation was performed with AutoDock 1.5.6 software and Pymol software assessed the protein-ligand complex and intermolecular interactions[9]. The vibrational data and the modes were allocated based on the potential energy distribution (PED) acquired from the Veda 04 tool. The optimal structure, vibrational frequencies, and HOMO-LUMO energies are computed using the B3LYP 6-311 ++ G (d, p) basis set. To achieve satisfactory agreement, the computed wavenumber data are compared with the experimental data. The Multiwfn 3.7 application was used to accomplish Electron Localization Function (ELF), and Localization Orbital Locator (LOL) along with VMD programs at reduced density gradient (RDG) [10].

Result and Discussion

GC-MS analysis

The gas chromatography-mass spectrometry analysis of a methanol extract of *Hybanthus enneaspermus* containing the medicinal component 3MBD-TMC is shown in (Fig. 1). The analysis reveals the molecular weight to be 208.18 g/mol, the retention period to be 42.22 min, and the molecular formula to be $C_{14}H_{24}O$. The bio-component accessible data is well-correlated with these findings and can be found in the PubChem databases and NIST data repository. Based on its anticancer properties, the molecule fared well in comparison experiments on 3MBD-TMC using quantum chemical computation, spectroscopic analysis and molecular docking[11].

Optimized Molecular Structure

The optimized molecular structure of cyclohexanol is depicted in (Fig. 2), showcasing the spatial arrangement of atoms within the molecule. The optimized geometrical parameters, including bond lengths and bond angles, were obtained using the

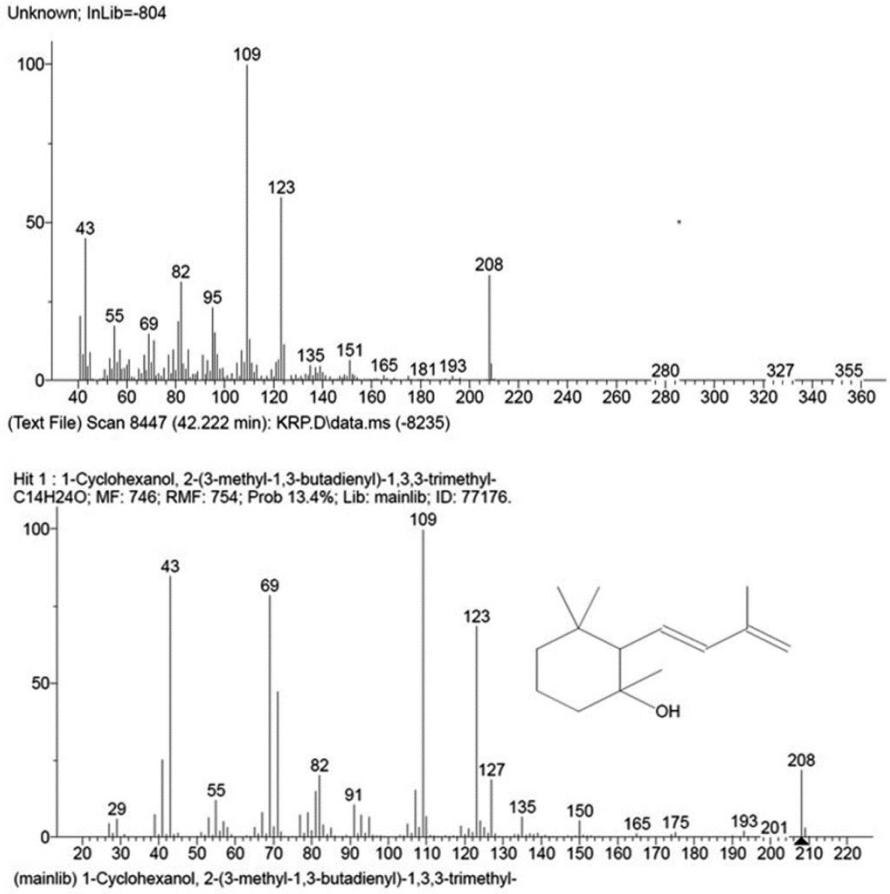

Fig. 1 — Gas chromatography-mass spectrometry analysis of 3MBD-TMC

Density Functional Theory (DFT) method and are systematically presented in (Table 1), derived from the calculated values[12]. The title molecule is composed of fourteen carbon atoms, one oxygen atom, and twenty-three hydrogen atoms, forming a complex yet well-defined structure. Table 1 highlights the key bond lengths within the molecule, where the C_1-C_2 and C_2-C_3 bonds are observed to have the longest bond lengths, measuring 1.58 Å and 1.57 Å, which is well correlated to the experimental values of 1.53 Å, 1.51 Å, respectively. C_2-H_{16}, and C_4-H_{17} have a bond length of 1.098 Å and 1.097 Å with XRD Values depicted as 1.080 Å, and 1.010 Å These extended bond lengths may indicate areas of relative flexibility or strain within the cyclohexanol structure. Conversely, C_1-O_7 with a 1.432 Å value matched the

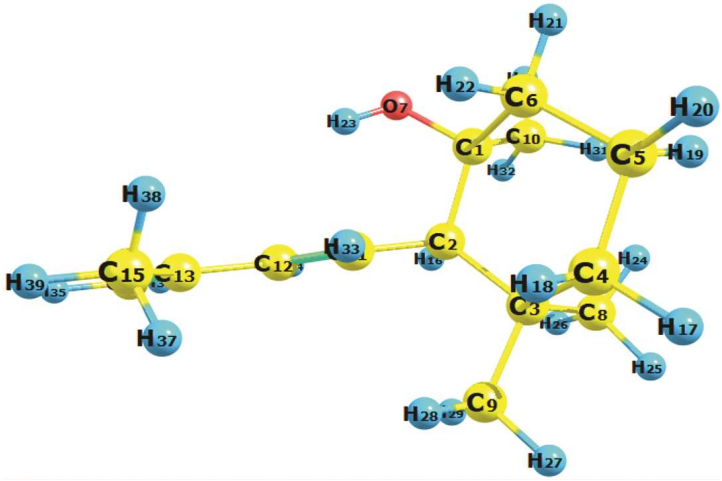

Fig. 2 — Optimized structure of 3MBD-TMC

Table 1 — Bond length (Å) and Bond angle (Degree) of the 3MBD-TMC compound

Bond Length	Values	Experimental	Bond Length	Values	Experimental
C_1-C_2	1.58	1.53	C_8-H_{25}	1.09	0.93
C_1-C_6	1.54	1.4	C_8-H_{26}	1.09	1.21
C_1-O_7	1.43	1.41	C_9-H_{27}	1.09	0.96
C_1-C_{10}	1.53	1.45	C_9-H_{28}	1.09	0.98
C_2-C_3	1.57	1.51	C_9-H_{29}	1.09	0.98
C_2-C_{11}	1.51	1.48	C_{10}-H_{30}	1.09	1.09
C_2-H_{16}	1.09	1.00	C_{10}-H_{31}	1.08	0.96
C_3-C_4	1.55	1.55	C_{10}-H_{32}	1.09	0.93
C_3-C_8	1.54	1.58	C_{11}-C_{12}	1.34	1.32
C_3-C_9	1.54	1.5	C_{11}-H_{33}	1.08	1.1
C_4-C_5	1.53	1.56	C_{12}-C_{13}	1.46	1.45
C_4-H_{17}	1.09	0.91	C_{12}-H_{34}	1.09	0.99
C_4-H_{18}	1.09	0.9	C_{13}-C_{14}	1.34	1.4
C_5-C_6	1.53	1.53	C_{13}-C_{15}	1.50	1.5
C_5-H_{19}	1.09	0.95	C_{14}-H_{35}	1.08	-
C_5-H_{20}	1.09	0.99	C_{14}-H_{36}	1.08	-
C_6-H_{21}	1.09	0.95	C_{15}-H_{37}	1.09	1.01
C_6-H_{22}	1.09	0.95	C_{15}-H_{38}	1.09	-
O_7-H_{23}	0.96	1.03	C_{15}-H_{39}	1.09	0.98
C_8-H_{24}	1.08	0.99			
C_2-C_1-C_6	109.9	109.1	C_3-C_8-H_{26}	110.9	109
C_2-C_1-O_7	109.2	107.1	H_{24}-C_8-H_{25}	107.0	107
C_2-C_1-C_{10}	113.9	112.9	H_{24}-C_8-H_{26}	107.6	107.8
C_6-C_1-O_7	109.6	109.1	H_{25}-C_8-H_{26}	107.4	106.2
C_6-C_1-C_{10}	111.3	112.5	C_3-C_9-H_{27}	110.0	109
O_7-C_1-C_{10}	102.4	101.3	C_3-C_9-H_{28}	112.4	109
C_1-C_2-C_3	114.7	115.6	C_3-C_9-H_{29}	111.1	111

(*Contd.*)

Table 1 — Bond length (Å) and Bond angle (Degree) of the 3MBD-TMC compound — (*Contd.*)

Bond Length	Values	Experimental	Bond Length	Values	Experimental
C_1-C_2-C_{11}	109.2	107.9	H_{27}-C_9-H_{28}	107.7	109.5
C_1-C_2-H_{16}	106.4	108.2	H_{27}-C_9-H_{29}	107.7	107.2
C_3-C_2-C_{11}	110.9	109.7	H_{28}-C_9-H_{29}	107.4	107.9
C_3-C_2-H_{16}	107.9	106.8	C_3-C_8-H_{24}	113.7	-
C_{11}-C_2-H_{16}	107.1	-	C_3-C_8-H_{25}	109.6	-
C_2-C_3-C_4	109.8	-	C_1-C_{10}-H_{30}	107.6	107.8
C_2-C_3-C_8	111.7	-	C_1-C_{10}-H_{31}	113.5	-
C_2-C_3-C_9	109.6	109.4	C_1-C_{10}-H_{32}	110.9	109.4
C_4-C_3-C_8	110.3	-	H_{30}-C_{10}-H_{31}	107.9	-
C_4-C_3-C_9	108.9	108.1	H_{30}-C_{10}-H_{32}	107.8	106.9
C_8-C_3-C_9	106.0	107.5	H_{31}-C_{10}-H_{32}	108.7	108.2
C_3-C_4-C_5	114.1	112.4	C_2-C_{11}-C_{12}	124.4	-
C_3-C_4-H_{17}	108.8	-	C_2-C_{11}-H_{33}	116.8	112.5
C_3-C_4-H_{18}	109.0	108.1	C_{12}-C_{11}-H_{33}	118.6	120.3
C_5-C_4-H_{17}	110.1	-	C_{11}-C_{12}-C_{13}	126.3	-
C_5-C_4-H_{18}	108.5	109	C_{11}-C_{12}-H_{34}	118.3	118.2
H_{17}-C_4-H_{18}	105.7	-	C_{13}-C_{12}-H_{34}	115.3	-
C_4-C_5-C_6	111.6	112.9	C_{12}-C_{13}-C_{14}	119.6	119.6
C_4-C_5-H_{19}	110.1	-	C_{12}-C_{13}-C_{15}	118.9	117
C_4-C_5-H_{20}	109.4	-	C_{14}-C_{13}-C_{15}	121.3	120.1
C_6-C_5-H_{19}	109.9	108.2	C_{13}-C_{14}-H_{35}	121.7	119.8
C_6-C_5-H_{20}	109.6	-	C_{13}-C_{14}-H_{36}	121.4	120.3
H_{19}-C_5-H_{20}	105.7	-	H_{35}-C_{14}-H_{36}	116.7	-
C_1-C_6-C_5	113.3	-	C_{13}-C_{15}-H_{37}	111.2	111.1
C_1-C_6-H_{21}	108.6	108.7	C_{13}-C_{15}-H_{38}	111.2	-
C_1-C_6-H_{22}	108.2	-	C_{13}-C_{15}-H39	111.1	-
C_5-C_6-H_{21}	111.0	-	H37-C15-H_{38}	106.8	107.9
C_5-C_6-H_{22}	109.2	-	H_{37}-C_1-H_{39}	108.0	107.1
C_{12}-C_6-H_{22}	106.1	105.8	H_{38}-C_{15}-H_{39}	108.0	107.8
C_1-O_7-H_{23}	107.5	109.5			

XRD value of 1.410 Å, the functional group attached to the cyclohexanol through C_1-O_7 bond linked asO_7-H_{23} bond, which exhibits the shortest bond length, recorded at 0.968 Å, reflecting the strong interaction between the oxygen and hydrogen atoms, typical of hydroxyl groups in alcohols. These geometrical insights provide a deeper understanding of the molecular structure and the nature of bonding within the cyclohexanol molecule with an RMSD value of the bond length of 0.1029Å, and bond angle of 1.3353˚ where good values represent the sign for further studies. Likewise, the bond angle between the Carbon, Oxygen, and Hydrogen of the title compound expressed with the combination of angles obtained C_2-C_1-O_7, C_6-C_1-O_7, O_7-C_1-C_{10}, along with both DFT as 109.2°, 109.6°, 102.4°and experimental values matched as per this 107.1°, 109.1°, 101.3°. In C_{11}-C_{12}-C_{13}, C_{14}-C_{13}-C_{15} possess the values 126.3°, 121.3° correlated to the XRD Values 121.6°, 120.1°. C_2-C_{11}-H_{33}, C_{15}-H_{39} have 116.8°, 111.2° match to the experimental values 112.5°, 111.1° and the H_{31}-C_{10}-H_{32}, H_{30}-C_{10}-H_{32} have well matched with both the experimental and DFT values 108.7°/108.2°, 107.8°/106.9°, respectively[13].

Mulliken atomic charges, MEP surface and PES analysis

The electron density determines the Mulliken atomic charges. In the field of quantum mechanical calculations for molecular systems, the charge distribution of the molecules is very important. The charge distribution across the atoms affects several properties of molecular systems, such as the electronic structure, molecule polarizability, and dipole moment. Also, several chemical reaction mechanisms, such as electronegativity equalization and charge transfer, have been described in terms of atomic charge. The Mulliken population analysis of the title compounds was done at the B3LYP/6-311++G (d, p) level to acquire atomic charge values. It clearly shows that the charge of carbon atoms C_{12} has the highest negative charge of -0.097 eV and C_1 has the highest positive charge of 0.282 eV. Three atoms, H_{22}, C_2, and O_7, are connected to C_1, which has a strong positive charge because of their influence. The Mullikan atomic charges are mentioned in (Table 2)[14].

Table 2 — Mulliken Atomic Charges of 3MBD-TMC

Atoms	Charges (eV)	Atoms	Charges (eV)
C_1	0.282	C_{21}	0.095
C_2	-0.082	C_{22}	0.077
C_3	0.033	C_{23}	0.294
C_4	-0.166	C_{24}	0.099
C_5	-0.190	C_{25}	0.095
C_6	-0.174	C_{26}	0.098
C_7	-0.571	C_{27}	0.093
C_8	-0.304	C_{28}	0.097
C_9	-0.298	C_{29}	0.098
C_{10}	-0.307	C_{30}	0.116
C_{11}	-0.134	C_{31}	0.093
C_{12}	-0.097	C_{32}	0.102
C_{13}	0.177	C_{33}	0.088
C_{14}	-0.292	C_{34}	0.084
C_{15}	-0.380	C_{35}	0.094
C_{16}	0.079	C_{36}	0.097
C_{17}	0.086	C_{37}	0.120
C_{18}	0.083	C_{38}	0.116
C_{19}	0.092	C_{39}	0.110
C_{20}	0.090		

Molecular electrostatic potential MEP is a helpful technique for characterizing the reactivity, hydrogen bonding, and structure of molecular behaviors[15]. The 3D plot of the Molecular Electrostatic Potential (MEP) is presented in (Fig. 3a), it was calculated from B3LYP/6-311++G (d, p) basis set with the Gauss View program 5.0. The charge appropriations on molecules are depicted in three dimensions using MEP. The MESP is a useful tool for understanding how molecules interact, helping predict things like bonding, solvent effects, and reactive sites. Different colours correspond to the various sections of the MEP plot. The colours blue and red denote nucleophilic and electrophilic reactivity, respectively. The colour coding of the current molecule is between -5.611e^{-}2 (red) and +5.611e^{-}2 (blue). Since the red surfaces have high electron densities, they are connected to nucleophilic sites. Similarly, low electron density and electrophilic sites are indicated by colours blue. Meanwhile, green surfaces indicate areas with no potential. The Potential Energy Surface (PES) graph helps show how a molecule's energy changes with its shape, making it useful for studying stability, reactions, and light-sensitive materials. Using the PES scan surface in (Fig. 3b) calculated by the HF/6-311++G (d, p) software, the conformational flexibility of the 3MBD-TMC structure has been assessed[16]. Based on the local minimum energy that occurred in the PES scan plot report, as illustrated in (Fig. 3), the torsion angle of O15–C1–C3–H19 in tetrahydro

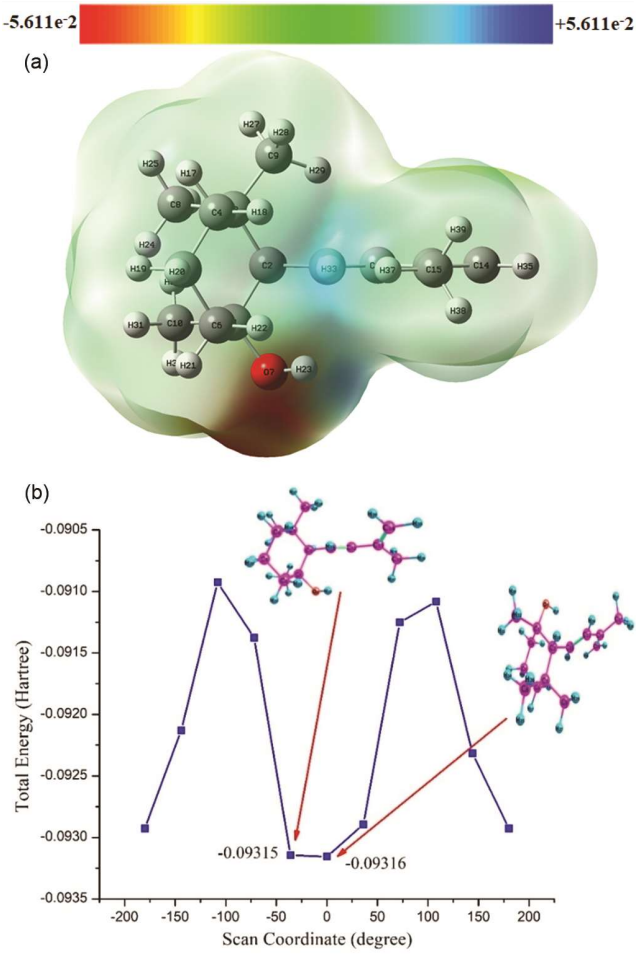

Fig. 3 — (a) MEP Map Surface on 3MBD-TMC Compound; (b) PES of 3MBD-TMC Compound

determines stability and instability in the 3MBD-TMC molecules[17]. The energy fluctuation in a molecule as a function of a dihedral angle—the angle between two planes made up of four atoms in succession—is depicted by a dihedral PES (Potential Energy Surface) graph. When examining the rotational conformations of flexible molecules, such as butane or ethane, where rotations around single bonds result in several energy states, this kind of PES is very helpful. The X-axis represents the dihedral angle, which is usually between 0° and 360°. The torsional rotation about a single bond is represented by this angle. The Y-axis displays the molecule's potential energy at each dihedral angle, showing how the energy varies with bond rotation. The PES graph frequently displays recurring peaks (greater energy) and dips (lower energy) as the angle increases from 0° to 360° because dihedral angles are periodic. The dihedral angle of title molecules flips at 10 steps on

each scan, revealing several conformers at 360◦. At the 0◦ and -36◦ scan coordinator, a local minimum energy curve with -0.09138, -0.09315 total energy (Hartree) was seen, suggesting a more to-ground state of the system. A less stable conformation on 3MBD-TMC molecules is shown by the torsional angle (C11-C12-C13-C14) of the local maximum energy curve which conformed at -108.00, 108.00 scan coordinates with -0.09093, -0.09108 Hartree energy.

Vibrational Assignments

The vibrational spectrum assignments for the title molecule, consisting of 39 atoms and 111 normal modes of vibration, were made based on experimentally recorded FT-IR spectra. These assignments were further supported by anticipated wavenumbers obtained using the density functional B3LYP/6-311++G (d, p) technique. The molecule, which exhibits C1 point group symmetry, has all its vibrational modes active in both infrared and Raman spectra. The calculated and experimental values are presented in the accompanying table for comparison (Table 3). To gain deeper insights into the vibrational characteristics, the force fields were calculated and used to determine the vibrational potential energy distribution (PED) with the VEDA 4 program[18]. This approach allowed for a detailed analysis of the vibrational modes, providing a comprehensive understanding of the molecular vibrations in the title compound. Figure 4 displays the theoretical and real FT-IR spectra of the 3MBD-TMC molecule.

CH Vibrations

C-H stretching vibrational bands are usually reported between 3100-3000 cm^{-1}[1,19]. The CH stretching vibrations in the studied compound are observed at 3070 cm^{-1}, 3049 cm^{-1}, and 3000 cm^{-1}in the experimental FT-IR spectrum. The corresponding computational values obtained using Density Functional Theory (DFT) with the B3LYP/6-311++G (d, p) basis set are 3075 cm^{-1}, 3039 cm^{-1}, and 3023 cm^{-1}. The close agreement between the experimental and computational values, with deviations of 5 cm^{-1}, 10 cm^{-1}, and 23 cm^{-1}, respectively, indicates that the theoretical method accurately captures the vibrational characteristics of the CH groups. The Potential Energy Distribution (PED) analysis shows contributions of 92%, 94%, and 89% for these modes, respectively, confirming that they are predominantly CH stretching vibrations with minimal mixing from other modes. This alignment of experimental and computational data highlights the robustness of the computational approach in analyzing the vibrational properties of the CH bonds in the molecule.

CH_2 Vibrations

CH2 vibrations are allocated to peaks between 2550 cm-1 and 3500 cm^{-1}. Hydrogen bonding plays a part in the broadening[20]. The CH^2 vibrational analysis reveals a strong correlation between the experimental spectral data and the computational predictions made using the DFT/B3LYP/6-311++G (d, p) basis set level. Specifically, the CH_2 stretching vibration calculated at 3243 cm^{-1} matches closely with the FTIR value of 3239 cm^{-1} with a PED contribution of 100%, indicating a pure stretching mode. Additionally, another CH_2 stretching mode is observed with a computational value of 3144 cm^{-1} which aligns perfectly with the corresponding FT-IR value of 3144 cm^{-1} and shows a PED of 94%. These results demonstrate that the experimental spectral data is well matched with the computational model, confirming the accuracy and reliability of the DFT method for predicting vibrational behavior in CH_2 groups.

CH_3 Vibrations

The anti-symmetric and symmetric stretching modes of methyl groups are typically observed between 3100 and 2880 cm^{-1}[21]. In this study, the methyl group stretching mode is evident at 3098 cm−1 in the FT-IR spectra, which closely matches the computational value of 3101 cm^{-1} obtained using the DFT/B3LYP/6-311++G (d, p) basis set level. The PED analysis shows a contribution of 99% for this mode, confirming its strong vibrational character associated with the CH_3 group. The excellent agreement between the experimental and computational spectral data further validates the accuracy of the DFT method in predicting the vibrational properties of methyl groups in this region.

The UV-Visible spectrum of the title compound was recorded experimentally with different solvents such as gas, and dimethyl sulfoxide (DMSO), Which is measured in the 200-300 nm range these are displayed in (Table 4 and Fig. 5). The UV-visible (UV-Vis) spectrum of the molecule was analyzed using (Time-dependent density functional theory) TD-DFT/B3LYP/6-311++G (d, p) technique. The computational results identified three significant excited states, each characterized by specific absorption bands, excitation energies, oscillator strengths, and major electronic transitions[24].

Table 3 — Experimental Data and Theoretical Frequencies/PED Calculated by Veda

B3LYP/ 6-311++G (d, p)	FT-IR	Vibrational Assignments + (PED%)	B3LYP/6-311++ G (d, p)	FT-IR	Vibrational Assignments + (PED%)
3570	3552	υOH (100)	1362	-	δHCC (60)
3243	3239	$\upsilon CH_{2\,(}$100)	1345	1350	δHCC (44)
3171	-	υCH (88)	1319	1300	δHCC (25)
3165	-	υCH (95)	1292	1280	τHCCC (18)
3175	-	υCH (95)	1282	-	δHCC (30)
3152	-	υCH (90)	1263	-	δHCC (32)
3144	3144	υCH2 (94)	1242	1240	δHCC (20) + υCC (11)
3134	-	υCH (95)	1207	-	δHCC (27) + υCC (12)
3130	-	υCH (97)	1188	-	δHCC (23)
3123	-	υCH (92)	1153	1151	υCC (11)
3107	-	υCH (99)	935	-	υCC (10)
3101	3098	υCH3 (99)	1138	-	δHCC (42) + υCC (12)
3089	-	υCH (99)	1103	1100	υCC (10)
3083	-	υCH (92)	1080	1080	δHCC (43)
3075	3070	υCH (92)	1074	1080	δHCC (53) + τHCC (12)
3064	-	υCH (88)	1065	-	υCC (30)
3061	-	υCH (82)	1045	-	τCCC (29)
3048	-	υCH (86)	1018	1000	τHCCC (35) + τHOCC (12)
3039	3049	υCH (94)	1382	-	δHCC (20)
3038	-	υCH (78)	1009	1005	δHCC (19)
3037	-	υCH (95)	998	980	δHCC (39)
3031	-	υCH (91)	373	-	υCC (10)
3029	-	υCH (95)	959	-	δHCC (15)
3023	3000	υCH (89)	951	946	υCC (13)
1713	-	υCC (60)	947	-	υCC (38)
1337	-	υCC (24) + δHCC (38)	572	550	υCC (13) + τHCCC (13)
1671	1672	υCC (70)	924	-	τHCCC (90)
1459	1450	υCC (12) + δHCC (68)	914	902	υCC (37)
1536	1540	δHCH (62)	895	-	δHCC (12)
1524	-	δHCH (47)	859	850	δHCC (34)
1519	-	δHCH (59)	881	-	υCC (36)
1513	1500	δHCC (63) + τHCCC (21)	842	840	υCC (61)
1512	-	δHCH (58)	774	-	δHCC (13)
1508	-	δHCH (55)	722	718	δHCC (17)
1506	1503	δHCH (72)	708	-	τHCCC (72)
1497	-	δHCH (55)	615	-	δHCC (40)
1494	1495	δHCH (69)	548	530	δHCC (26) + τHCCC (14)
1492	-	δHCH (78)	526	-	δHCC (15)
1441	1440	δHCC (64)	493	500	τHCCC (26)
1424	-	δHCC (74)	473	-	τHCCC (29)
1416	1412	δHOC (52)	459	451	δHCC (16)
1396	-	δHCC (32)	446	-	δHCC (16)
1381	1380	δHCC (38)	425	420	δCCC (24)
1373	-	δHCC (25)	410	401	δHCC (20) + τHOCC (17)

The UV-visible spectra of the compound in both DMSO and gas phases reveal similar electronic transitions. The Conjugated systems transition in the UV-Vis band exhibits stronger and more efficient absorption because of the smaller energy gap between π-π∗. In DMSO, the first major absorption peak occurs at 243.33 nm with an oscillator strength of 0.653, primarily due to a HOMO to LUMO transition (74%). A second peak at 228.99 nm (oscillator strength 0.2854) involves a HOMO-1 to LUMO transition (74%). A third weak peak at 197.58 nm corresponds to a HOMO-2 to LUMO n-π∗ transition (89%). In the gas phase, comparable transitions are observed at 242.51 nm, 228.56 nm, and 197.57 nm with similar contributions and the experimental absorption peak 241nm well correlated with the obtained value for the DMSO, Gas phase. The consistent peaks across both phases suggest that the compound's electronic structure is stable and not significantly influenced by the solvent[25].

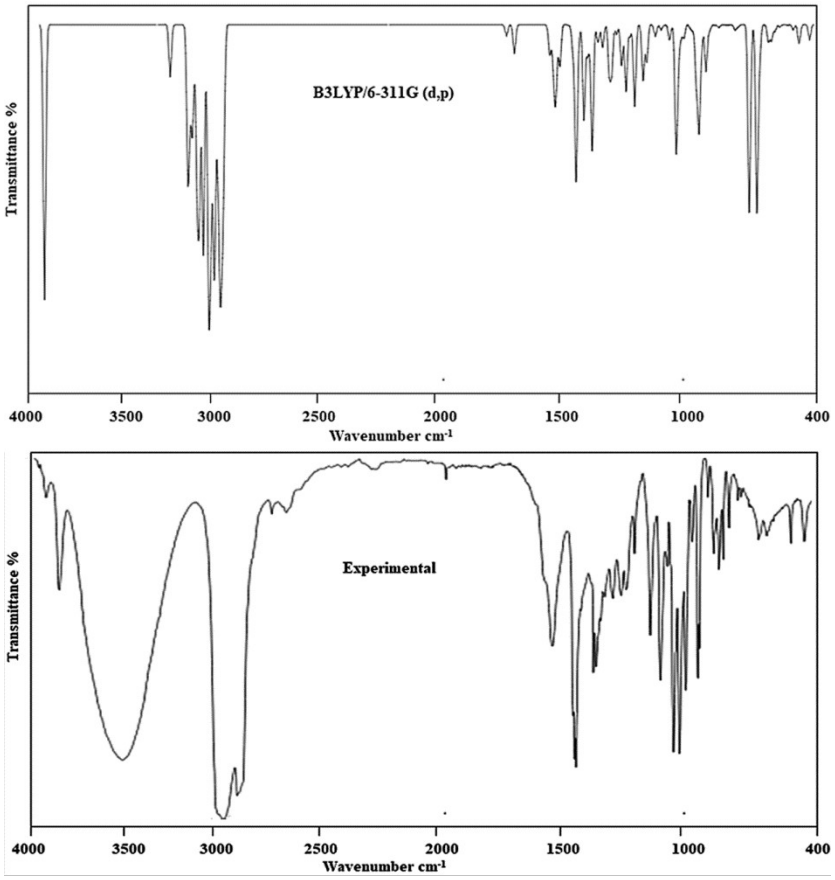

Fig. 4 — Compared FT-IR spectrum and theoretical spectrum on 3MBD – TMC

Table 4 — Electronic excitations of 3MBD – TMC obtained by TD-DFT/B3LYP/6-311++G (d, p) methods

State	B3LYP/6-311++G (d, p) Absorption Band λ (nm)	Excitation Energies (eV)	Oscillator Strength	Major Contributions Energy (%)	Experiment (nm)
DMSO					241
S1	243.33	5.10	0.6530	H-1->LUMO (26%), HOMO->LUMO (74%)	
S2	228.99	5.42	0.2854	H-1->LUMO (74%), HOMO->LUMO (25%)	
S3	197.58	6.28	0.0055	H-2->LUMO (89%) H-5>LUMO (7%)	
Gas Phase					
S1	242.51	5.12	0.6112	H-1->LUMO (29%), HOMO->LUMO (71%)	241
S2	228.56	5.43	0.3088	H-1->LUMO (71%), HOMO->LUMO (28%)	
S3	197.57	6.28	0.0057	H-2->LUMO (89%) H-5>LUMO (7%)	

OH Vibration

Hydroxyl bonds stabilize molecular structures and increase stretching frequencies when force constants change. Intramolecular hydrogen bonding occurs in the hydroxyl group, with stretching vibrations anticipated at 3590-3400 cm^{-1}[1,22]. The OH stretching vibration in the studied compound is observed at 3552 cm^{-1} in the experimental FTIR spectrum, while the computational analysis using Density Functional Theory (DFT) with the B3LYP/6-311++G (d, p) basis set predicts this mode at 3570 cm^{-1}. The minimal deviation of 18 cm^{-1} between the experimental and theoretical values indicates the accuracy of the computational method. Potential Energy Distribution (PED) analysis reveals a 100% contribution

from the OH stretching mode, confirming its localization and purity. This close alignment between experimental and computational results underscores the theoretical approach's reliability in capturing the OH group's vibrational characteristics.

CC Vibrations

Typically, C = C and C - C stretching vibrations in aromatic compounds exhibit bands ranging from 1430 cm^{-1} to 1650 cm^{-1}[1,23]. The analysis of C–C and C=C vibrational modes shows good agreement between the experimental FT-IR data and the computational values obtained using the B3LYP/6-311++G (d, p) method. The C– C stretching vibration, with a computational value of 1459 cm^{-1} corresponds closely with the observed FT-IR peak at 1450 cm^{-1} indicating a reliable prediction. Similarly, the C=C stretching vibration is calculated at 1242 cm^{-1} and matches the experimental FTIR value of 1240 cm^{-1}. It can be shown that the computational predictions and the experimental data correlate well because these vibrational modes lie within the expected range for C–C and C=C stretching frequencies. This alignment between theory and experiment confirms the accuracy of the B3LYP/6-311++G (d, p) method for predicting vibrational characteristics, satisfying the expected values for these functional groups.

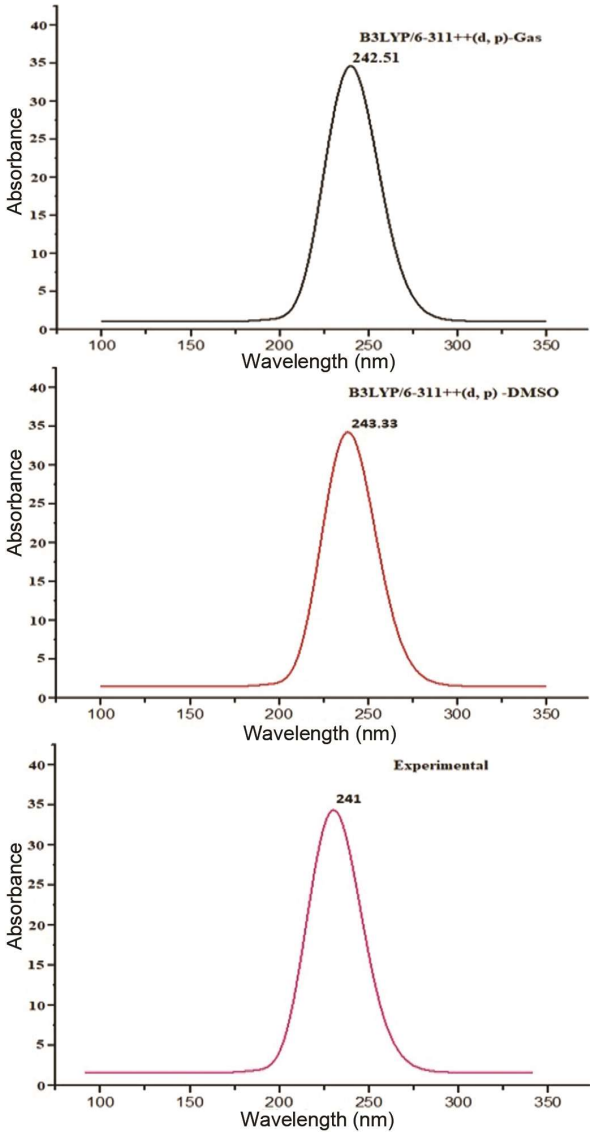

Fig. 5 — UV -visible analysis of 3MBD – TMC

UV -Visible Analysis

Frontier molecular orbital (FMO) studies

An essential idea in quantum chemistry is the Frontier Molecule Orbital (FMO), which aids in the analysis of a 3MBD-TMC chemical structure as an electronic property, including Δ Nmax (EV), chemical hardness, chemical softness, electrophilicity index, nucleophilicity index, electron donor power, electron acceptor power, ionization potential, electron affinity, electro negativity, and chemical potential. By examining the HOMO and LUMO, scientists can gain valuable insight into the behavior and characteristics of molecules, aiding in understanding their reactivity and stability in different environments. This information is crucial for predicting how a molecule may interact in chemical reactions and its potential applications in various fields. Using the DFT/B3LYP method with a specific basis set (6-311++G (d, p) to calculate the frontier molecular orbitals (FMO) of the molecule under study[26]. Table 5 lists the characteristics mentioned. Figure 6 Shows the HOMO, with an energy of 6.136 eV, donating electrons to the LUMO, which has an energy of 0.718 eV, resulting in an energy gap of 5.418 eV. This analysis helps us understand the chemical reactivity and stability of the molecule. Therefore, in this case, the title compound is considered chemically stable based on its energy gap exceeding 5ev[27]. Several novel chemical reactivity descriptors have been proposed to better understand various areas of pharmacological sciences, such as drug design and potential eco-toxicological properties of drug compounds. Chemical hardness, calculated to be 2.7.9 ev, supports the stability of the molecule, whereas electronegativity, which describes the ability to induce shared electrons, is found to be -3.427 ev. The high electrophilicity index of 4.335 ev emphasizes biological activity, demonstrating a pathway for molecular docking with several proteins. The scope of

Table 5 — Chemical stability & reactivity on 3MBD - TMC molecules

Electronic Properties	Values (eV)	Electronic Properties	Values (eV)
E_{HOMO} (eV)	6.136	Chemical hardness	2.709
E_{LUMO} (eV)	0.718	Chemical softness	0.369
E_{HOMO}–E_{LUMO} (eV)	5.418	Electrophilicity Index	4.335
Ionization potential	-6.136	Nucleophilicity Index	0.230
Electron affinity	-0.718	Electron donor power	-4.219
Electronegativity	-3.427	Electron acceptor power	0.626
Chemical potential	3.427	ΔN_{max} (EV)	1.265

the compound in medical and industrial applications is represented by the chemical softness value, which is found to be 0.369 eV demonstrating the harmless nature of the substance[28]. The title compounds 3MBD-TMC global reactive descriptors were computed using HOMO and LUMO values are shown below Ionization potential IP = -6.136, Electron affinity EA = -0.718, Electronegativity X = -3.427, Chemical potential μ = 3.427, chemical hardness η = 2.709, chemical softness 1/ η = 0.369 electrophilicity index ω = 4.335, nucleophilicity index 1/ω = 0.230, electron donor power (ω^+) = - 4.219, Electron acceptor power (ω^-) = 0.626, ΔN_{max} (EV) = 1.265.

NBO Analysis

Natural Bond Orbital (NBO) analysis of the 3MBD-TMC molecule was performed using the NBO 3.1 program in Gaussian 09 W software at the B3LYP/6-311++G (d, p) level of theory. This analysis provides a robust framework for evaluating maximal electron density and electron delocalization within the molecular orbital system[29]. The utilization of NBO analysis is very beneficial in examining areas with elevated electron density, evaluating the stability of molecules as a result of hyper conjugative interactions and charge delocalization, and comprehending interactions between and within molecules[30]. The strength of interactions between donor and acceptor orbitals can be quantified using the second-order perturbation energy (E^2) or stabilization energy (E^2). Higher stabilization energies indicate stronger interactions between the donor and acceptor orbitals, correlating with increased adsorption capabilities of the sensing material[31]. The perturbation energies derived from the interactions between donor (i) and acceptor (j) orbitals are presented in (Table 6). Notably, the interactions σ (C13-C14) → σ* (C11-C12) and σ (C11-C12) → σ* (C13-C14) exhibit stabilization energies of 23.81 Kcal/mol and 42.72 Kcal/mol, respectively. These results indicate a significant interaction between these orbital pairs, underscoring the molecule's stability and electron delocalization characteristics.

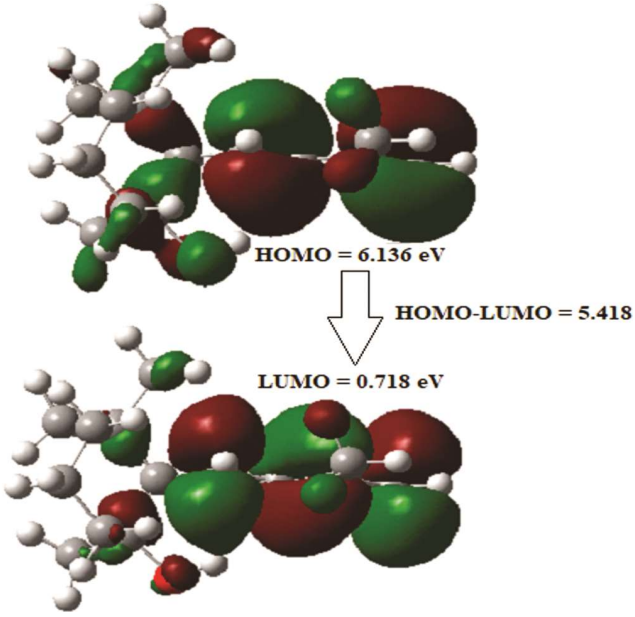

Fig. 6 — HOMO-LUMO energy values for 3MBD – TMC

Topology analysis for real space functions

Topological analysis helps to characterize and forecast the molecular structure of molecules, as well as providing a model for understanding how aetheric wave functions of atoms should fit together. The theory of atoms in molecules gives an effective answer for splitting molecular properties into contributions from atoms or functional groups[32]. Figure 2 shows the Optimized geometrical structure.

Electron localization function (ELF)

ELF stands for Electron Localization Function is used to analyze the charge transmission mechanism, aromaticity, shell structure, and the development of chemical bonds between atoms in organic small molecules. It also indicates the regions of atoms and molecules where electrons are most likely to be found, emphasizing areas such as lone pairs and chemical bonds[33]. A wave analyzer program Multiwfn 3.7 binwin64 software is used to create maps of ELF, denoted τ (r), and to analyze electronic wave functions

Table 6 — Selected second-order perturbation theory analysis of Fock matrix in NBO basis of 3MBD – TMC

Donor	Acceptor	E (2) Kcal/mol	E (j) – E (i) a. u.	F (i, j) a. u.
σ C_4 - H_{18}	σ* C_5 - H_{19}	2.85	0.91	0.046
σ C_2 - H_{16}	σ* C_{11} - H_{33}	3.70	0.95	0.053
σ C_{12} - C_{13}	σ* C_{11} - C_{12}	4.92	1.40	0.074
σ C_{12} - H_{34}	σ* C_{13} - C_{15}	5.94	0.94	0.067
σ C_{14} - H_{36}	σ* C_{13} - C_{15}	6.44	0.94	0.070
σ C_{13} - C_{14}	σ* C_{11} - C_{12}	23.81	0.31	0.077
σ C_{11} - C_{12}	σ* C_{13} - C_{14}	24.72	0.32	0.080

(Fig. 7). The colour indicators range from blue to red, showing ELF values from (0.0 to 1.0) [34]. However, the red area suggested n-localization whereas the blue area indicated n-delocalization electrons like oxygen, hydrogen, and carbon atoms[35].

Localized orbital locator (LOL)

Since both LOL and ELF rely on kinetic energy density, they are similar. ELF is based on the electron pair density, whereas (LOL) Localized orbital locator only notes that the localized orbitals' gradients are largest when the localized orbitals overlap[36]. This is a very effective method for understanding biochemical bonding between atoms in a compound. LOL, assessment ranges from 0.000 and 0.800[37] (Fig. 8). The colour red denotes a higher LOL ranking, whereas blue represents a lesser LOL ranking. A low LOL value confirms the presence of delocalized electrons.

Electron-hole analysis

Density Functional Theory (DFT) is a key method in studying these materials' electronic structures, offering detailed insights into the distribution of electrons and holes.Heat maps are visual tools derived from DFT results that show where electrons and holes are located in a system. These maps simplify complex quantum data, making it easier to analyze charge distribution, electronic transitions, and material behavior.The distribution of electronic states within a material across various energy levels is depicted by the Density of Surface Heat Map[38]. A compound's energy bands can be represented in two dimensions using a band structure. Concentrations of electrons are found in places with high charge densities, whereas holes are found in regions with low densities. Analyzing charge density reveals information about electron and hole spatial distributions and interactions. Through the interpretation of heat maps in hole-electron analysis inside DFT. It provides information about the electrical properties of different materials by interpreting heat maps in hole-electron analysis within DFT[39]. Charge transfer excitation of

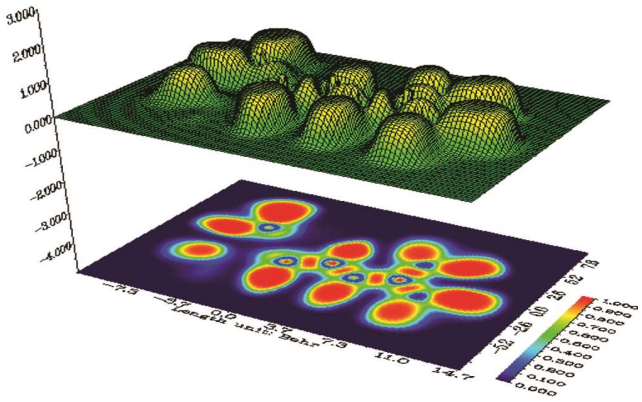

Fig. 7 — Electron localized function (ELF) map of 3MBD-TMC

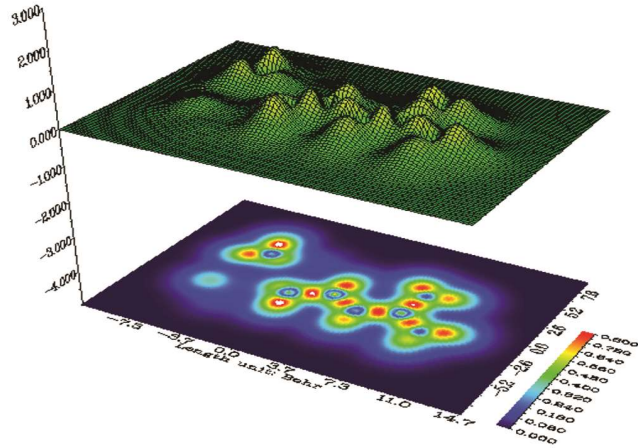

Fig. 8 — Localized orbital locator (LOL) map of 3MBD-TMC

states I, II, and III is revealed by studies of the hole-electron interaction. Investigating the charge transfer resulting from excitation can help to better understand how the HOMO-LUMO gap contributes to intramolecular charge transfer. For each excitation mode, the Dr index, overlap integral, and charge transfer length may be determined. The B3LYP/6-311G approach is used to optimize the molecule and perform a TDDFT calculation, while also offering a very comprehensive insight into all forms of electron transfer features and their investigation of electron excitation qualities.Utilizing Multiwfn 3.7, a very

large and powerful tool to do electron excitation analysis, the isosurface electron-hole analysis plots (green-blue) and overlap of electron-hole distribution were completed in (Fig. 9). In 3MBD-TMC, there are–OH, –CH3 groups (electron donors) on one side of its structure and a π linker (benzene) on the other. This method is quite useful for identifying the type of electron excitations. Analysis of electron holes (Fig. 10). shows three overlapping energy excitation states[40]. Together with the distributions of holes C2, C3, H26, C8, C3, O7, and electrons C11, C12, C13, and H36 are present in the initial excitation state. Comparably, the electron and hole distribution in the second excitation state was represented by the blue C2, C3, C8, O7, and the green C14, C13, C12, C11, H36, and H29. In the third state, electron distribution occurs at C11, C12, C13, C14, and H36 with hole distribution H27, H29, H32, and C8 as in previous states.O7 is a red-colored symbol that represents an OH group overlap in the electron-hole distribution in III state.The number of atoms allocated to each Gaussian09 atom is indicated on the heat map's X-axis. The energy contribution is indicated by the color scale on the right. Its Y-axis represents the electron, hole, and overlap, respectively[41]. The isosurface correlatesC11, C14 in I state to red on the heat map to depict an electron with an energy of 0.324 Å, while the blue C2, C3 indicate an absence hole and only overlap the electron population in the I state. The sky blue C1, C3 represent the holeswith an energy level of 0.19 Å, while the other black mark on the map indicates the lack of holes. The overlap at I state at C11 represents an energy level of 0.195 Å. The crowding of electrons in the I state causes the II state of C11, C12, C13, and C14 of isosurface correlate to transition to red, orange, and light green on the heat map, representing electrons with 0.324 Å energy levels. The remaining black and blue indicate the distribution of holes with lower energy levels. The hole distribution with 0.195 Å energy is represented by the C13 sky-blue, C11 red in the electron distribution with 0.065 Å, and 0.324 Å with C14 green. C11, C12, C13, and C14 overlap with 0.130 Å, 0.195 Å, and 0.259 Å energy levels at II stage of

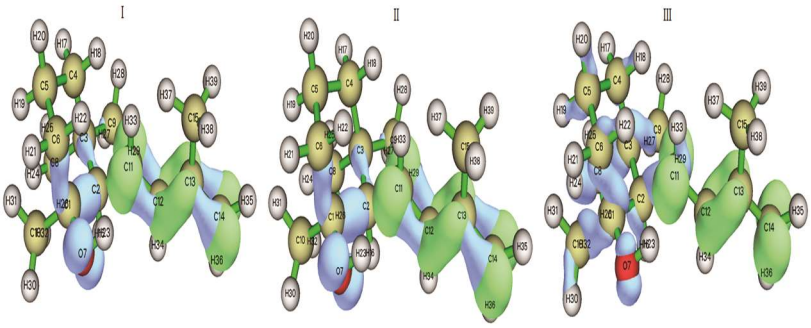

Fig. 9 — Electrons and Holes distribution diagrams of all excited states in 3MBD-TMC

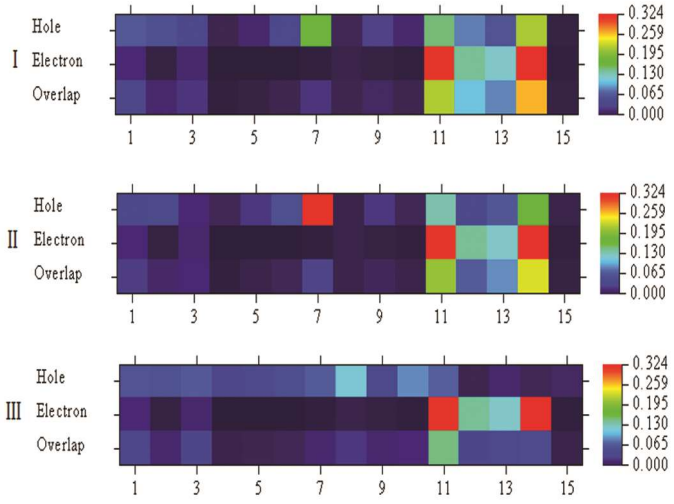

Fig. 10 — Electron-hole analysis of I→III transition in the visible light region for3MBD-TMC

excitation.On the heat map, the 0.130 Å energy on the holes distribution at III state is indicated by the overlapping of I and II, which produced the C11, C14 red color as an electron holder with 0.324 Å of isosurface correlated with C8 sky-blue. When comparing the above energy states, C11 overlaps at an energy level of 0.130 Å. In condition III, the other blue mark on the map indicates the absence of electrons and overlaps[42].

Reduced density gradient (RDG) analysis

In order to forecast the intermolecular interaction based on the electron density, Reduced density gradient (RDG) was a crucial study. The compound's noncovalent interaction was determined by its beneficial biological feature[43]. Since electron density and this method are closely related, they both start from the same fundamental idea interactions ought to be able to be studied exclusively using electron density[44]. The low electron area is characterized by calculating the low-density gradient, which is concerned with weak contact, whereas the high-density gradient value is utilized to pinpoint strong interaction. The color-filled RDG map and scatter map of the header composite were plotted with Multiwfn 3.7. analyser[45]. Thus, the approach may differentiate hydrogen bonding, van der Waals, and repulsive steric interactions using simple colour codes. Figure 11 shows three colours green, red, and blue in our molecules stand for Van Der Waals, steric effect (repulsive), and H-bond interactions. Organic unit atoms exhibit the repulsive interaction (red zone), which has a significant steric influence. There is a positive sign in this region (λ2) ρ between 0.01 and 0.05 a.u. The hydrogen atom in the organic group demonstrates van der Waals contact (the green zone). There is another van der Waals contact found in the chemical under study between the organic and inorganic groups. At the sign area of (λ2) ρ = 0, the van der Waals interaction takes place. Furthermore, the figure's dark blue patches, which resemble O-H, show a strong hydrogen bond between the group's hydrogen and nitrogen atoms. This robustly attractive link lies between -0.02 and -0.05 a.u. and has a negative sign (λ2) ρ[46].

Nuclear Magnetic Resonance Of 3MBD-TMC

In Physics, chemistry, biology, and medicine, Nuclear magnetic resonance (NMR) is a potent analytical method that is frequently employed to ascertain the dynamics and structure of molecules.

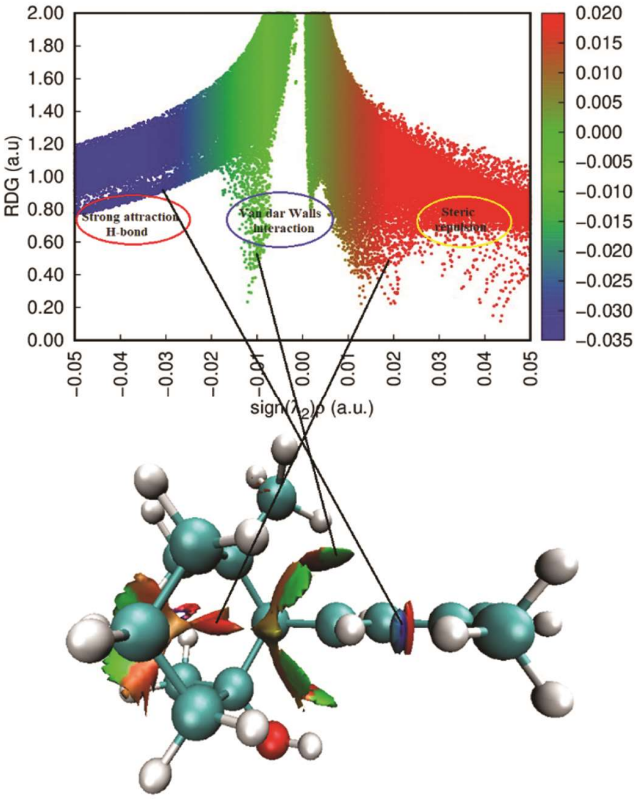

Fig. 11 — Visual Representation of RDG Analysis in 3MBD-TMC

The way 1D 1H, 13C and 2D NMR spectra NMR operate is by subjecting a sample to a powerful magnetic field, which alters the magnetic nuclei of atoms like carbon (^{13}C) and hydrogen (^{1}H). These nuclei absorb energy and realign when a radiofrequency pulse is introduced. They release signals when they return to their initial condition, which is picked up and converted into an NMR spectrum. The spectrum's chemical shifts provide information on the molecular structure, such as the spatial arrangement and bonding between atoms[47]. NMR is particularly helpful for investigating protein structures, detecting chemical compounds, and even imaging tissues for medical purposes like magnetic resonance imaging (MRI). It is an essential tool in many scientific fields because of its non-destructive nature and capacity to offer comprehensive information on molecular environments. Table 7 displays the title compound's theoretical chemical shift values for the carbon (13C) and proton (1H) NMR. Because it shows the hydrogen and carbon skeletons, the NMR is a great tool for determining the structure of an organic complex. The GIAO technique is used to predict the theoretical chemical shifts for ^{1}H and ^{13}C from B3LYP/6–311++G (d, p) [48]. Methylene,

Table 7 — NMR of 3MBD-TMC

Atom	Theoretical chemical shift in ppm	Experimental chemical shift in ppm	Atom	Theoretical chemical shift in ppm	Experimental chemical shift in ppm
C_1	44.680	44.503	H_{21}	7.762	7.71
C_2	7.207	7.431	H_{22}	5.594	5.02
C_3	9.455	-	H_{23}	15.684	-
C_4	21.759	24.491	H_{24}	13.309	-
C_5	8.010	-	H_{25}	7.845	7.73
C_6	20.367	-	H_{26}	8.323	-
O_7	67.638	67.521	H_{27}	9.374	-
C_8	11.525	12.212	H_{28}	8.113	-
C_9	47.390	45.565	H_{29}	5.897	5.01
C_{10}	15.385	14.240	H_{30}	8.698	-
C_{11}	153.599	-	H_{31}	6.506	6.89
C_{12}	118.226	-	H_{32}	14.733	-
C_{13}	168.995	168.282	H_{33}	14.416	-
C_{14}	103.252	-	H_{34}	8.443	-
C_{15}	18.760	-	H_{35}	6.969	6.91
H_{16}	3.502	3.35	H_{36}	7.026	7.59
H_{17}	7.396	7.61	H_{37}	11.124	11.16
H_{18}	6.042	-	H_{38}	8.268	-
H_{19}	6.754	-	H_{39}	8.117	-
H_{20}	10.610	10.14			

which is joined to the remainder of the molecule by a carbon-carbon double bond, is represented by the Carbon (C14) peak at 103.252 ppm. The OH functional group at the C1 which is at 44.680 ppm / 44.503 ppm at the end of the benzene ring and the C5 methylene group at 8.010 ppm. The Methylene group at the C3 end of the benzene ring is represented by the peak (C8, C9) at 11.525 ppm, 47.390 ppm, whereas the Methylene group at the C4 and C6 ends of the benzene ring is represented by the peaks at 21.759 ppm, 20.367 ppm. It was anticipated that the protons on the carbon of a methyl group would exhibit chemical shift values between 0.6 and 1.5 parts per million. A carbon atom in a distinct environment inside the molecule is identified by each peak. Because the carbons are in two distinct environments, there are peaks in this instance[49]. Three hydrogen atoms and a carbon atom are joined to form the CH3 group. Two hydrogen atoms—a carbon and an oxygen atom—are joined to the carbon in the CH2 group. The theoretical chemical shift of 1H that has been observed ranges from 3.502 to 11.124 ppm. Figure 12 shows the compound 3MBD-TMC observed 1H and 13C NMR spectra. Because it has a stronger electronegative atom attached, the CH2, CH3 group is responsible for the greater chemical shift. In the peaks and its corresponding values of the C-H chemical shift in 3MBD-TMC, the H_{21} with 7.762 / 7.71 ppm; H_{22} with 5.594 / 5.02 ppm, H_{35} with 6.969 / 6.91 ppm; H_{36} with 7.026 / 7.59 ppm match with the both the theoretical and experimental which is placed in the benzene ring at C_6, C_{14} to form the methyl group, the C_{11};C_{12}, C_{13};C_{14} the largest ppm values represent the double bond C=C in 3MBD-TMC, whose presence is confirmed by the computed chemical shift and experimental NMR values of methylene and methyl, respectively with corresponding experimental values matched to the theoretical values of the title compound 3MBD-TMC.

Molecular docking and Protein-ligand interaction analysis

In this study, the Auto Dock Tool 1.5.6 application was employed to perform molecular docking, providing insights into the fundamental biological mechanisms and predicting the interactions between small molecules and the binding site of a target protein[50,51]. The target protein, identified as 8D58, was obtained from the Protein Data Bank (PDB) and downloaded in PDB format for the docking procedure. The ligand 3MBD-TMC was synthesized and its structure was generated using MolView.org for compatibility with the PDB format[51-55]. The binding interaction between the ligand and the 8D58 receptor was characterized by a notable binding affinity, with a maximum negative binding energy of -5.13 kcal/mol, as demonstrated in (Table 8). The docking results highlighted the involvement of GLU 202 in the formation of a hydrogen bond (H…O) with the ligand, which contributed to the stability of the ligand-protein complex. The estimated inhibition

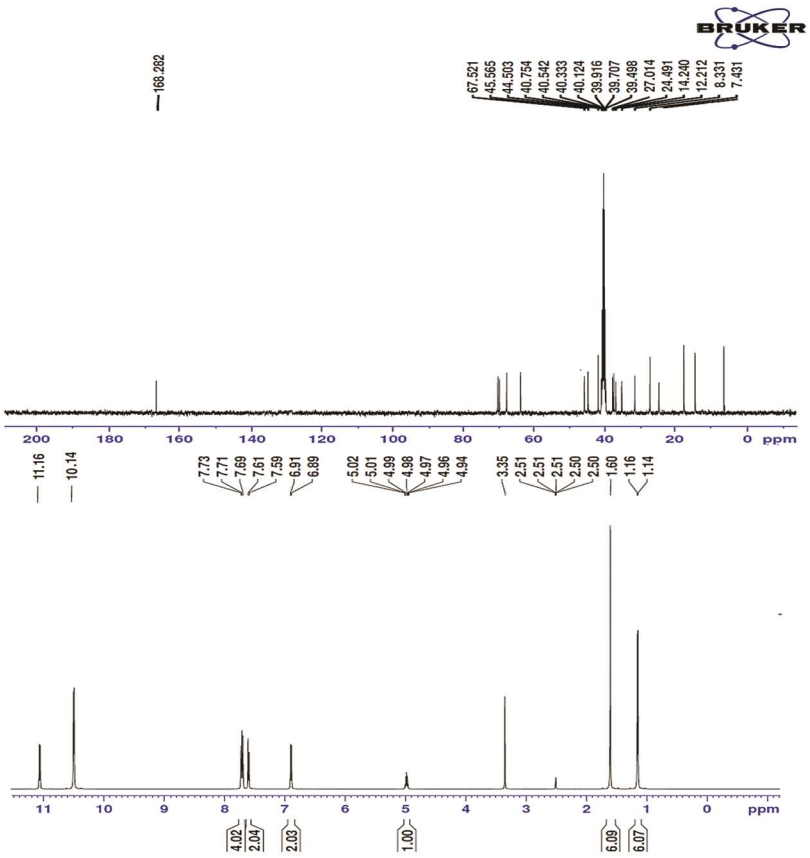

Fig. 12 — ^{13}C NMR &^{1}H NMR of 3MBD-TMC

Table 8 — The Binding affinity of the proteins with RMSD value on CMIO

Ligands	Protein (PDB ID)	Bonded residues	No. of hydrogen bond	Bond distance (Å)	Estimated Inhibition Constant (μ m)	Binding energy (kcal/mol)	Reference RMSD (Å)
3MBD-TMC	8D58	GLU 202 (H…O)	1	1.7	172.59	- 5.13	81.02

constant for the interaction was calculated to be 172.59 μ m, and the reference Root Mean Square Deviation (RMSD) value was found to be 81.02 Å, indicating a reliable docking score. Furthermore, as illustrated in (Fig. 13).

The title compounds exhibited potent inhibitory activity against the (crystal structure of human METTL1-WDR4 complex) 8D58 receptor, which is associated with *Candida albicans*, as evidenced by the formation of a stable ligand-protein association characterized by a single hydrogen bond with a distance of 1.7 Å. These findings suggest that the 3MBD-TMC molecules demonstrate strong binding energy and effective inhibition of the 8D58 receptor, positioning them as promising candidates for further development in antifungal therapies. The quality of the protein structure was assessed using a Ramachandran plot, which confirmed the protein's integrity and suitability for the docking study [56,57]. Figure 14 shows that relatively few residues are found in prohibited regions and that 90% of the residues are found in the red, darkest zone. For a protein model consisting of 557 residues, a Ramachandran plot analysis was conducted to evaluate the quality of the structural model. By examining whether the ϕ\phi and ψ\psiψ angles of the amino acids fall within the permitted regions, Ramachandran plots are used to validate protein structures. It aids in comprehending the flexibility and conformational stability of certain protein domains. The analysis was benchmarked against 118 reference structures, each with a resolution of at least 2.0 Å and an R-factor no greater than 20.0%. According to established standards, a high-quality model is expected to have over 90% of residues in the most favored regions, specifically regions. This benchmark serves as a critical indicator

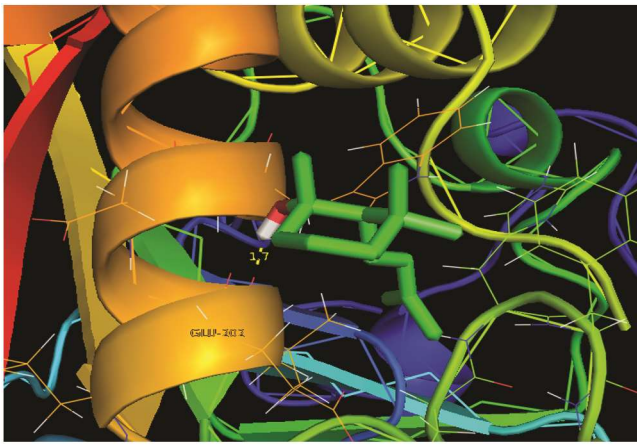

Fig. 13 — Molecular docking studies of 3MBD-TMC with 8D58 protein

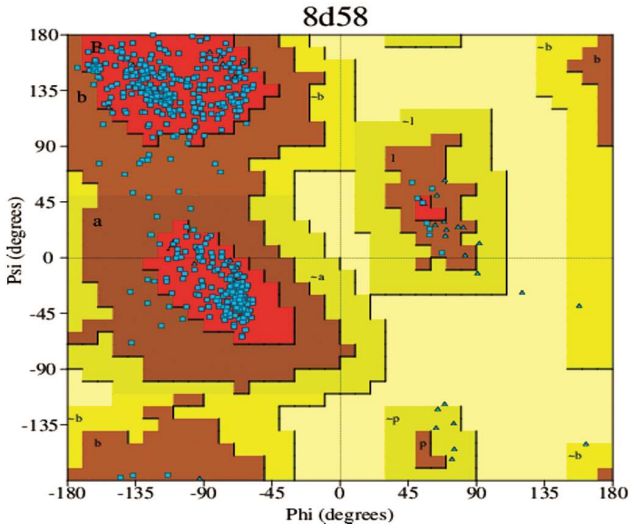

Fig. 14 — Ramachandran plots of 8D58 protein

of the model's reliability and accuracy in representing the protein's conformational space.

Conclusion

The optimum structure from the optimized geometry for the title compound 3MBD-TMC, the increased bond length (Å) and bond angle (◦) were attained at C_1-C_2 (1.58Å), C_{11}-C_{12}-C_{13} (126.3◦) derived from the structure in the current study. Through the use of the Gaussian program 09W and the B3LYP functional DFT calculation. It was accurately determined how a solvent affected the electrical characteristics in FMO and MEPS. The MEP map indicates that the oxygen atoms have negative potential sites, whereas the hydrogen atoms have positive potential sites around them. The PES scan and potential energy of the dihedral torsional angles in different rotations exhibit the strength and flexibility of the 3MBD-TMC compound. The HOMO–LUMO energy gap value of 5.418 eV was linked to notable chemical reactivity, per NBO studies. To support the derivation conclusion, each unique normal mode vibration was compared and characterized using the simulated FT-IR spectra. PED% agreement between the calculated frequencies and the FT-IR spectra was good. The absorption peaks found in the UV-Vis electronic spectra (λ_{max} = 242.51 nm) and DMSO (λ_{max} = 243.33 nm) show a good contrast to the UV-Vis spectra (λ_{max} = 241 nm). With a stronger electronegative atom attached, the CH2, CH3 groups exhibit the shift in NMR, which results in the greater chemical shift or the carbon peak (C_1) at both experimental and theoretical44.680 ppm / 44.503 ppm representing the OH functional group presence at the NMR studies. The electron-hole heat maps and electron-hole distribution diagrams of electrons and holes in all excited states provide a comprehensive understanding of the atomic and molecular states of binding nature through the characteristics of electrons and holes. The electron zones of localization and delocalization were identified by this assessment. Using Multiwfn software, the wave functions—the electron localized function (ELF), localized orbital locator (LOL), and non-covalent interaction (RDG) —were evaluated. Molecular docking simulations have also been utilized to determine the minimum binding energies of protein targets 8D58 to the ligand 3MBD-TMC, which are - 5.13 kcal/mol, respectively. Protein structures are verified by the use of Ramachandran plots. The METTL1-WDR4 complex is capable of killing cancer cells, contributes to carcinogenesis, and can be effectively targeted in cancer therapy.

Conflict of interest

All authors declare no conflict of interest.

References

1 Anushya S & Shanthi P, Pharmacological, phytochemical screening and evaluation of in vitro anticancer potential of traditional medicinal plant *Morinda umbellata* L. leaf extracts on human breast carcinoma MCF 7 cell line. *Res J Biotech*, 17 (2022) 111-117.

2 Sapnakumari M, Divya K, Aswin KB & Dalin J, Antimicrobial and Antioxidant Study of Some Newly Synthesized Chalcones and Cyclohexenone Derivatives. *Asian J Chem*, 35 (2023) 114.

3 Shin SY, Park J, Jung Y, Lee YH, Koh D, Yoon Y & Lim Y, Anticancer activities of cyclohexenone derivatives. *Appl Biol Chem*, 63 (2020) 82.

4 Abdullah MN, Osw P, Hassan SA & Othm S, Two new cyclohexenone derivatives: Synthesis, DFT estimation,

biological activities and molecular docking study. *J Mol Struct*, 1301 (2024) 222.

5 Uddin N, Rashid F, Haider A, Tirmizi SA, Raheel A & Imran M, Zaib S, Diaconescu PL, Iqbal J & Ali S, Triorganotin (IV) carboxylates as potential anticancer agents: Their synthesis, physiochemical characterization, and cytotoxic activity against HeLa and MCF-7 cancer cells. *Appl Organomet Chem*, 35 (2021) 4.

6 Manikandan A, Rajesh P, Prabakaran AR & Gunasekaran S, Spectroscopic and Quantum Chemical Calculations of 4- (2, 5-dichlorobenzyl) -2, 3, 4, 5, 6, 7-hexahydro-7- (4 methoxyphenyl) benzo[h] [1, 4, 7] triazecin-8 (1h) -one from leaves of Cassia auriculata (Avaram). *Int res j eng Tech*, 04 (2017) 184.

7 Prabhu C, Rajesh P, Vijayalakshmi D, Parthasarathy M, Dhanalakshmi E & Gowthami V, Kinetic Stability and Spectroscope investigation of Octadecanoic Acid- 17-Oxo-Methyl Ester (OA17OME). *Neuro Quantol*, 20 (2022) 2098.

8 Sevanthi S, Muthu S, Aayisha S, Ramesh P & Raja M, Spectroscopic (FT-IR, FT-Raman and UV-Vis), computational (ELF, LOL, NBO, HOMO-LUMO, Fukui, MEP) studies and molecular docking on benzodiazepine derivatives- heterocyclic organic arenes. *Chem Data Collect*, 30 (2020) 100574.

9 Rajesh P, Kandan P, Sathish S, Manikandan A, Gunasekaran S, Gnanasambandan T & Bala Abiramig S, Vibrational spectroscopic, UV-Vis, molecular structure and NBO analysis of Rabeprazole. *J Mol Struct*, 1137 (2017) 277.

10 Mohammed K, Mohammed AAK, Hakiem AFA & Mahfouz RM, Computational evaluation on the molecular conformation, vibrational spectroscopy, NBO analysis and molecular docking of betaxolol and betaxolol-chlorthalidone cocrystals. *J Mol Struct*, 1209 (2020) 127744.

11 Thendral ED, Gomathi S, Sumaya UM, Biruntha K & Usha G, 1- (Pyridin-2-yl) -2, 4-bis[(pyridin-2-yl) carbonyl]-3, 5-bis (3, 4, 5-trimethoxyphenyl) cyclohexanol 2.25-hydrate. *Acta Cryst*, 2 (2017) x171624.

12 Chandralekha K, Gavaskar D, Sureshbabu AR & Lakshmi S, 5′-Benzylidene-1″-methyl-4″-phenyl-trispiro[1,3-dioxolane-2,1′-cyclohexane-3′,3″-pyrrolidine-2″,3‴-indole]-4′,2‴-dione. *Acta Crystallogr B*, 73 (2017) 5.

13 Samshuddin S, Jasinski JP, Butcher RJ, Neuhardt EA, Narayana B, Yathirajan HS & Glidewell C, Three closely related cyclohexanols (C35H27X2N3O3; X = F, Cl or Br): similar molecular structures but different crystal structures. *Acta Crystallogr C*, 70 (2014) 953.

14 Prabhaharan M, Prabakaran AR, Srinivasan S & Gunasekaran S, Density functional theory studies on molecular structure, vibrational spectra and electronic properties of cyanuric acid. *Spectrochim*, 138 (2015) 711.

15 Ceylan U, Capan A, Yalcin SP, Sonmez M & Aygun M, Vibrational spectroscopic and thermodynamical property studies, Fukui functions, HOMO–LUMO, NLO, NBO and crystal structure analysis of a new Schiff base bearing phenoxy-imine group. *J Mol Struct*, 1136 (2017) 222.

16 Hollebeek T, Ho TS & Rabitz H, Constructing multidimensional molecular potential energy surfaces from ab initio data. *Annu Rev Phys Chem*, 50 (1999) 537.

17 Sevvanthi S, Muthu S, Raja M, Aayisha S & Janani S, PES, molecular structure, spectroscopic (FT-IR, FT-Raman), electronic (UV-Vis, HOMO-LUMO), quantum chemical and biological (docking) studies on a potent membrane permeable inhibitor: dibenzoxepine derivative. *Heliyon*, 6 (2020) 8.

18 Rajesh P, Gunasekaran S, Gnanasambandan T & Seshadri S, Experimental, quantum chemical and NBO/NLMO investigations of pantoprazole. *Acta*, 136 (2015) 247.

19 Arumugam T, Ramalingam A, Guerroudj AR, Sambandam S, Boukabcha N & Chouaih A, Conformation and vibrational spectroscopic analysis of 2,6-bis(4-fluorophenyl)-3,3-dimethylpiperidin-4-one (BFDP) by DFT method: a potent anti-Parkinson's, anti-lung cancer and anti-human infectious agent. *Heliyon,* 10 (2024) 30.

20 Vasanthakumari R, Nirmala W, Sagadevan CS, Mugeshini S, Rajeswari N, Ranjith Balue & Santhakumari R, Synthesis, growth, crystal structure, vibrational, DFT and HOMO, LUMO analysis on protonated molecule-4-aminopyridinium nicotinate. *J Mol Struct*, 239 (2021) 130449.

21 Rocha M, Di Santo A, Arias JM, Gil MD & Altabef AB, Ab initio and DFT calculations on molecular structure, NBO, HOMO–LUMO study and a new vibrational analysis of 4-(dimethylamino) benzaldehyde. *Spectrochim Acta A Mol Biomol Spectrosc*, 136 (2015) 130449.

22 Dexlin XDD, Tarika JDD, Kumar SM, Mariappan A & Beaula TJ, Synthesis and DFT computations on structural, electronic and vibrational spectra, RDG analysis and molecular docking of novel anti-COVID-19 molecule 3,5-dimethylpyrazolium 3,5-dichlorosalicylate. *J Mol Struct*, 1246 (2021) 131165.

23 Rajesh S, Gunasekaran S & Rajesh P, HOMO-LUMO, NBO and Vibrational analysis of Sitagliptin by using DFT calculations and Experimental Study (FT-IR, FTRaman and UV-Visible Spectroscopies. *Int J Chemtech Res,* 11 (2018) 107.

24 Mekoung PMA, Malloum A, Govindarajan M, Mballa RN, Patouossa I, Zintchem AAA, Nanseu CPN & Mbouombouo IN,Spectroscopic properties (FT-IR, NMR and UV) and DFT studies of amodiaquine. *Heliyon*, 9 (2023) 12.

25 Khemalapure S S, Katti V S, Hiremath C S, Hiremath S M, Basanagouda M & Radder S B, Spectroscopic (FT-IR, FT-Raman, NMR and UV-Vis), ELF, LOL, NBO and Fukui function investigations on (5-bromobenzofuran-3-yl)acetic acid hydrazide (5BBAH): experimental and theoretical approach. *J Mol Struct*, 1196 (2019) 280–290.

26 Antony I, John D, Jebaraj W, Jebasingh K & Sasitha T, DFT, NBO, HOMO–LUMO, NCI, stability, Fukui function and hole–electron analyses of tolcapone. *Comput Theor Chem*, 1202 (2021) 113296.

27 Rahuman MH, Muthu S, Raajaraman BR, Raja M & Umamahesvari H, Investigations on 2-(4-cyanophenylamino) acetic acid by FT-IR, FT-Raman, NMR and UV-Vis spectroscopy, DFT (NBO, HOMO–LUMO, MEP and Fukui function) and molecular docking studies. *Heliyon*, 6 (2020) e04976.

28 Vincy CD, Tarika JDD, Dexlin XDD, Rathika A & Beaula TJ, Exploring the antibacterial activity of 1,2-diaminoethane hexanedionic acid by spectroscopic, electronic, ELF, LOL, RDG analysis and molecular docking studies using DFT method. *J Mol Struct*, 1247 (2022).

29 Ojha JK, Ramesh G & Reddy BV, Structure, chemical reactivity, NBO, MEP analysis and thermodynamic

parameters of pentamethylbenzene using DFT study. *Chem Phys Impact*, 7 (2023) 100280.

30 Manjusha P, Prasana JC, Muthu S & Rizwana BF, Spectroscopic elucidation (FT-IR, FT-Raman and UV-visible) with NBO, NLO, ELF, LOL, drug likeness and molecular docking analysis on 1-(2-ethylsulfonylethyl)-2-methyl-5-nitroimidazole: an antiprotozoal agent. *Comput Biol Chem,* 88 (2020) 107330.

31 Adindu EA, Godfrey OC, Agwupuye EI, Ekpong BO, Agurokpon DC, Ogbodo SE, Benjamin I & Louis H, Structural analysis, reactivity descriptors (HOMO–LUMO, ELF, NBO), effect of polar (DMSO, EtOH, H_2O) solvation and libido-enhancing potential of resveratrol by molecular docking. *Chem Phys Impact*, 7 (2023) 100296.

32 Kazachenko AS, Tanis E, Akman F, Medimagh M, Issaoui N, Al-Dossary O, Bousiakou LG, Kazachenko AS, Zimonin D & Skripnikov AM, A comprehensive study of N-butyl-1H-benzimidazole. *Molecules*, 27 (2022) 7864.

33 Laura JJ, Rajesh P, Kesavan M, Dhanalakshmi E, Kayashrini S & Prabhaharan M, Degree–based topological indices, NMR chemical shifts, chemical reactivity, molecular dynamics and DFT analysis of 1, 4-Methanoazulene-9-methanol, Decahydro-4, 8, 8-trimethyl-, [1S- (1α, 3aβ, 4α, 8aβ, 9R)]. *Biophys Chem*, 322 (2025) 107442.

34 Vasanthi T, Balasubramanian V & Vijayakumar VN, Theoretical studies (DFT) on hydrogen bonded liquid crystal derived from 4-amino and 4-dodecyloxy benzoic acids. *Mater Today Proc*, 47 (2021) 1724.

35 Kayashrini S, Rajesh P, Dhanalakshmi E, Kesavan M, Prabhaharan M, Al Farraj DA & Elshikh MS, FT-IR,UV–Vis, density functional theory and molecular docking studies on 3, 7, 11, 15-Tetramethyl-2hexadecen-1-ol. *J Mol Struct*, 1321 (2025) 139600.

36 Rizwana BF, Prasana JC, Muthu S & Abraham CS, Molecular docking studies, charge transfer excitation and wave function analyses (ESP, ELF, LOL) on valacyclovir: a potential antiviral drug. *Comput Biol Chem*, 78 (2019) 9.

37 Subbaiah S, Elangovan N, Ajithkumar G & Manoj KP, (E)-4-((4-bromobenzylidene)amino)-N-(pyrimidin-2-yl) benzenesulfonamide from 4-bromobenzaldehyde and sulfadiazine: synthesis, spectral (FTIR, UV–Vis), computational (DFT, HOMO–LUMO, MEP, NBO, NPA, ELF, LOL, RDG) and molecular docking studies. *Polycycl Aromat Compd*, 42 (2022) 10.

38 Ding W, Xue Z, Li J, Li M, Bai L, Zhou Q, Zhou X, Peng Y & Miao L, Excited State Properties of Layered Two-Dimensional MSi2N4 (M = Mo, Cr, and W) Materials from First-Principles Calculations. *JSS,* 11 (2022) 016001.

39 Huang H, Li N, Fu S, Mo X, Cao X, Yin X & Yang C, Pure polycyclic aromatic hydrocarbon isomerides with delayed fluorescence and anti-kasha emission: High-efficiency non-doped fluorescence OLEDs. *Adv Sci*, 10 (2023) 2304204.

40 Zhang Y, Ma M, Shang C, Cao Y & Sun C, Theoretical Study on the Atom-Substituted Quinazoline Derivatives with Faint Emission as Potential Sunscreens. *ACS Omega*, 7 (2022) 14848.

41 Coetzee LC, Adeyinka A & Magwa N, A theoretical evaluation of the efficiencies of metal-free 1, 3, 4-oxadiazole dye-sensitized solar cells: insights from electron-hole separation distance analysis. *Energies,* 15 (2022) 4913.

42 Ila & Krishnamoorthy G, The suppression of intramolecular charge transfer emission by tautomerism in 2- (4′-amino-2′-hydroxyphenyl) -1H-imidazo-[4, 5-c] pyridine: Intramolecular proton transfer versus intermolecular proton transfer. *J Photochem Photobiol A,* 413 (2021) 113199.

43 Muthukumar R, Karnan M, Elangovan N, Karunanidhi M & Thomas R, Synthesis, spectral analysis, antibacterial activity, quantum chemical studies and supporting molecular docking of Schiff base (E)-4-((4-bromobenzylidene) amino) benzenesulfonamide. *J Indian Chem Soc*, 99 (2022) 100405.

44 Vedhapriya K, Balaji G, Dhiyaneshwari B, Irfan A, Thirunavukkarasu M, Kaleeswaran S, Rab SO & Muthu S, Effect of green solvents, molecular structure and topological studies on 4-amino-1-β-D-ribofuranosyl-1,3,5-triazin-2(1H)-one: anti-blood cancer agent. *J Indian Chem Soc*, 100 (2023) 100912.

45 Janani S, Rajagopal H, Sakthivel S, Aayisha S, Raja M, Irfan A, Javed S & Muthu S, Molecular structure, electronic properties, ESP map (polar aprotic and polar protic solvents) and topology investigations on 1-(tert-butoxycarbonyl)-3-piperidinecarboxylic acid: anticancer therapeutic agent. *J Mol Struct*, 1268 (2022) 133696.

46 Medimagh M, Ben Mleh C, Issaoui N, Kazachenko AS, Roisnel T, Al-Dossary OM, Marouani H & Bousiakou LG, DFT and molecular docking study of the effect of green solvent (water and DMSO) on the structure, MEP and FMOs of the 1-ethylpiperazine-1,4-diium bis(hydrogenoxalate) compound. *J Mol Liq*, 369 (2023) 120851.

47 Holland DC & Carroll AR, Structure Revision of Formyl Phloroglucinol Meroterpenoids: A Unified Approach Using NMR Fingerprinting and DFT NMR and ECD Analyses. *Molecules,* 29 (2024) 594.

48 Manwal P, Mekoung A, Malloum A, Govindarajan M, Mballa RN, Patouossa I, Abouem A Zintchem A, Nanseu CPN & Mbouombouo I N, Spectroscopic properties (FT-IR, NMR and UV) and DFT studies of amodiaquine. *Heliyon,* 9 (2023) 12.

49 Nardelli F, Borsacchi S, Calucci L, Carignani E, Martini F & Geppi M, Anisotropy and NMR spectroscopy. *Rendiconti Lincei*, 31 (2020) 999.

50 Kayashrini S, Rajesh P, Kesavan M, Kala A & Pavithra M, Application of Degree-Based Topological Descriptors, Molecular Properties, Chemical Reactivity Prediction and Nonlinear Optical Analysis of 5- [2- [4- (1, 2-benzothiazol-3-yl) piperazin-1-yl] ethyl]-6-chloro-1, 3-dihydroindol-2-one. *J Mol Struct*, 1354 (2025) 144847.

51 Laura JJ, Rajesh P, Kayashrini S & Abirami SB. Kojibiose as a Sustainable Bioactive Molecule: Experimental and DFT Insights into Antibacterial Activity and Electronic Properties. *J Mol Struct*, (2026) 145576.

52 Morris GM, Huey R, Lindstrom W, Sanner MF, Belew RK, Goodsell DS & Olson AJ, AutoDock4 and AutoDockTools4: Automated docking with selective receptor flexibility. *J Comput Chem*, 30 (2009) 2785.

53 Trott O & Olson AJ, AutoDock Vina: Improving the speed and accuracy of docking with a new scoring function, efficient optimization and multithreading. *J Comput Chem*, 31 (2010) 455.

54 Dhanalakshmi E, Rajesh P, Arunkumar K, Gnanasambandan T, Noureddine ISSAOUI, Sudha K & Raja M, Synthesis, GCMS, spectroscopic, electronic properties, chemical

reactivity, RDG, topology and biological assessment of 1- (3, 6, 6-trimethyl-1, 6, 7, 7a-tetrahydrocyclopenta[c]pyran-yl) ethenone. *Chem Phys Impact*, 7 (2023) 100385.

55 Dhanalakshmi E, Rajesh P, Kandan P, Kesavan M, Jayaraman G, Selvaraj A & Priya R, Stability of bonds, kinetic stability, energy parameters, spectral characterization, GC–MS and molecular descriptors studies on coumarine, 3- [2- (1-methyl-2-imidazolylthio) -1- oxoethyl]. *J Mol Struct,* 1295 (2024) 136544.

56 Lawrence M, Rajesh P, Ahmad Irfan & Muthu S, Importance of solvent roles in molecular, electronic and dynamical properties, thermodynamic quantities, Mulliken charges, reactive analysis and molecular docking of 2-Bromo-1H-imidazole-4, 5-dicarbonitrile. *J Mol Liq*, 388 (2023) 122744.

57 Alexandrov A, Martzen MR & Phizicky EM, two proteins that form a complex are required for 7-methylguanosine modification of yeast tRNA. *RNA*, 8 (2002) 1253.